Fusion-energy reaction ^{2}H(t,α)n from $E_t = 12.5$ to 117 keV

Nelson Jarmie, Ronald E. Brown, and R. A. Hardekopf
Los Alamos National Laboratory, Los Alamos, New Mexico 87545
(Received 13 March 1984)

We have measured the cross section for the important fusion-energy reaction ^{2}H(t,α)n at 17 energies over the triton bombarding energy range of 12.5—117 keV. This corresponds to an equivalent deuteron bombarding energy range of 8.3—78.1 keV and to a plasma temperature (kT) range of 0.7—18.8 keV. The cross section is accurate to 1.4% over most of the energy range, with the error rising to 4.8% at the lowest energy. These data are considerably more accurate than the previous d + t measurements in this energy range. We compare our data with those of other measurements and with an existing R-matrix analysis of the mass-5 system. We have also performed a single-level R-matrix analysis of a restricted data base that contains our data and have used that analysis to compute Maxwellian reactivities up to a plasma temperature of 20 keV. In addition, for calibration purposes, we measured to better than 1% absolute error the ^{2}H(p,p)^{2}H elastic differential cross section at six laboratory angles at a proton bombarding energy of 10.04 MeV.

I. INTRODUCTION

The ^{2}H(t,α)n reaction has long been of interest to both physicists and engineers. At low energies the reaction mechanism is dominated by a $J^\pi = \frac{3}{2}^+$ resonance, causing the cross section to peak at a value of about 5 b near a deuteron bombarding energy of 107 keV. With its 17.6-MeV Q value, this reaction has been used widely as a source of high-energy neutrons, and because of its high cross section at low energies, will certainly be the reaction used to fuel the first magnetic- and inertial-confinement fusion reactors that will eventually provide sufficient energy for commercial use. These reactors are expected to operate in the temperature range $kT = 1$—30 keV, which corresponds to laboratory bombarding energies having a large overlap with our range of 10—120 keV.

A recent evaluation[1] of past work on the d + t reaction[2–8] and of other nuclear reactions important for fusion energy indicated the possibility of large systematic errors in some of those experiments. In particular, it seemed[1] that beam-energy uncertainties caused by the use of foil-contained gas targets could have been a significant problem at these low energies where the reaction cross section changes very rapidly with incident energy. Therefore, part of the present technique is to use a thin, windowless, gas target to reduce to a low level the uncertainties due to beam energy losses.

In the present experiment we have used the low-energy fusion cross-section (LEFCS) apparatus, which is installed at the Los Alamos Ion Beam Facility. The LEFCS system was developed over the past several years and consists of the following major components: a 120-kV beam accelerating system, a windowless cryogenically pumped gas target, and a beam-power calorimeter. The entire LEFCS facility is described in detail in Sec. II.

In Sec. III the experimental procedures are described, and the results are presented in Sec. IV. There, it is seen that the ^{2}H(t,α)n cross section was measured at 17 triton bombarding energies from 12.5 to 117 keV, with relative errors of about 0.5% (except at the very lowest energies) and a scale error of 1.26%. In Sec. V we compare our measurements with those of others[2–8] and with an existing R-matrix analysis.[9] We also perform a single-level fit to a selected data base for deuteron bombarding energies up to 250 keV and use that fit to calculate reactivities for a Maxwellian d + t plasma up to a temperature kT of 20 keV. These reactivities are compared with previous results.[10–13] Concluding remarks are given in Sec. VI.

II. LEFCS FACILITY

In Fig. 1 we show a schematic diagram of the LEFCS system installed at the Los Alamos Ion Beam Facility. It is seen that particle beams from either a tandem Van de Graaff accelerator or a 120-kV source can be directed through a windowless cryogenically pumped target into a beam-power calorimeter. Discussions of some of the LEFCS apparatus have been given previously.[14–17]

A. 120-kV beam source

A 120-kV, dual-polarity ion source and accelerating system were built to Los Alamos specifications by the General Ionex Corporation. The ion source is a standard duoplasmatron with a 30-kV extraction lens, gridded einzel lens, and crossed-field analyzer. For the present experiment, which employs a triton beam, we operated the source in its negative-ion, direct-extraction configuration to produce pure ^{3}H$^-$ beams of 30—40 μA. Although positive beams of greater intensity can be produced, the use of ^{3}H$^-$ avoids possible contamination of a ^{3}H$^+$ beam with other mass-3 species, such as ^{3}He$^+$, ^{1}H$_3^+$, and ^{1}H^{2}H$^+$. Because of the beam collimation used to obtain good transmission through the target, the beam intensity at the target is reduced to about 10 μA at the higher energies and 2 μA at the lower energies.

 ©1984 The American Physical Society

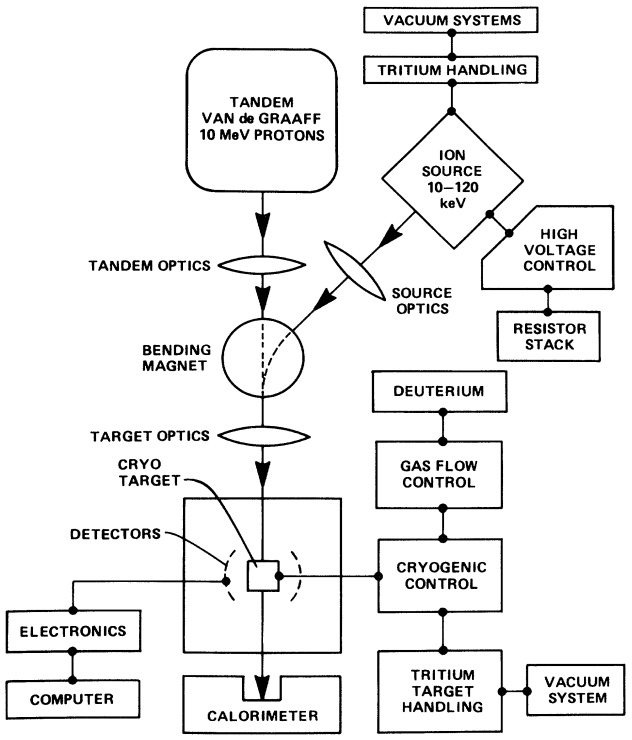

FIG. 1. Schematic diagram of the Los Alamos low-energy fusion cross section (LEFCS) facility.

The accelerating tube is a low gradient multielectrode structure providing low optical strength coupling to ground potential. The final beam energy is defined by a highly stable 120-kV power supply between the duoplasmatron and ground. This system allows the beam energy to be altered without affecting the extraction mechanism, and thus the beam current available and the terminal focusing are insensitive to beam energy over a broad range. Our tests have established that the accelerating voltage is stable to one part in 10^4 (FWHM) up to 100 kV, with the instability then rising from 10 V at 100 kV to 25 V at 120 kV. The absolute voltage is measured to better than one part in 10^4 with a 10^5 to 1 resistive divider (Spellman model HVD-200) whose calibration is traceable to the National Bureau of Standards.

The beam, which is diverging as it exits the accelerating tube, is focused by an einzel lens to a minimum beam waist at a position beyond the exit of a 45° double-focusing analyzing magnet. This magnet bends the ion beam onto the target-chamber axis, which is also the axis of the beam line from the tandem Van de Graaff accelerator. The beam size is delimited by a set of four-way slits at the waist position and then focused into the target chamber by another einzel lens. Complete optical control, necessary for good transmission, is obtained with electrostatic and magnetic steering devices at appropriate locations between the ion source and target. In particular, vertical steering plates before the 45° magnet are electrically biased to act as an astigmatic lens to correct for optical distortions introduced by the 45° magnet. Beam currents of 1.4 to 4 μA were used in the present experiment, although more intense beams were available at the higher beam energies.

The tritium gas used in the ion source is recirculated with a 500-l/s turbomolecular pump backed by a small mercury diffusion pump having a forepressure tolerance of at least 20 Torr. The tritium flow is regulated to maintain a constant pressure in the arc region of the duoplasmatron. Many of the details are similar to those in Ref. 18. An enclosed tritium collection system is located nearby, and when the ion source is shut down, the tritium is absorbed into charcoal-filled cylinders kept in dewars of liquid nitrogen.

B. Target and detection system

The target system is a substantially modified version of one obtained from Duke University.[19,20] A schematic diagram of this target, as modified, is shown in Fig. 2. To keep systematic errors arising from beam energy uncertainties at a low level, there are no gas-confining foils in the beam path. Instead, the $^2H_2$ target gas flows out through the beam ports, and about 98% is frozen onto

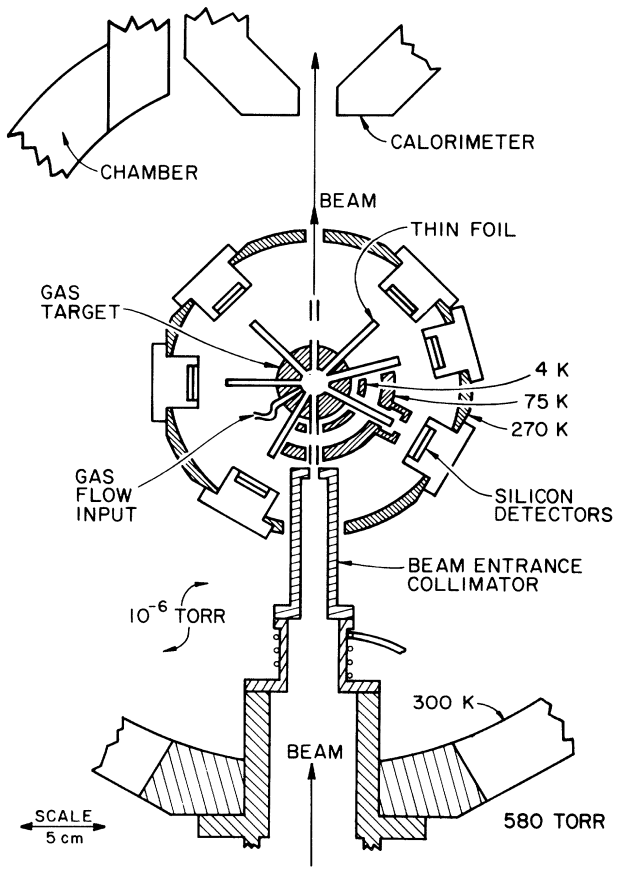

FIG. 2. LEFCS gas target and detector system. Only a portion of the 4-K and 75-K cylindrical surfaces are shown. The entrance collimator and the target are electrically isolated, and the currents are monitored.

surfaces that surround the central target region and are kept at a temperature of 4 K by a liquid-helium dewar. The remaining few percent is pumped by a 500-l/s turbomolecular pump. A liquid-nitrogen-cooled cylinder surrounds the 4-K pumping surfaces for thermal shielding. The central target region consists of a copper cooling container kept near 10.5 K and situated just below the 1-cm diameter main reaction volume. The $^2H_2$ gas, precooled to liquid-nitrogen temperature, flows at a rate of about 5 std-cm^3/min into the 10.5-K cooling region and then up into the reaction volume and out the beam ports. These operating conditions yield a target density of about 1.4×10^{16} ^2H atoms/cm^3 (a gas temperature, pressure, and areal density of about 35 K, 25 mTorr, and 0.01 μg/cm^2, respectively). In the $^2H(t,\alpha)n$ experiments, this density causes the total energy loss in the target to be in the range of only 70—190 eV. The cooling container temperature of 10.5 K was chosen to be only 1 K above the freezing point of deuterium at the target pressure used. This cooling helps to maximize the gas density for a given flow rate. The temperature of 10.5 K is maintained by the combination of resistive heating and liquid-helium cooling through a stainless steel thermal gradient rod and is measured with a germanium resistor connected via a standard four-wire system to a 10-μA constant current source and a digital voltmeter whose output was read by an on-line computer every 12 s. With a slope of 35 $\Omega\,K^{-1}$, the resistor provided a very sensitive and reproducible measurement. The temperature was stable enough that only infrequent manual adjustment of the heating-resistor current was necessary. Several figures in Refs. 19 and 20 give a reasonably good idea of the geometry of the target cryogenics, even after our modifications.

The flow rate of deuterium gas is set by adjustment of a fine needle valve fed by a buffer volume whose constant pressure is regulated by an automatic feedback control system. The analog output of a flowmeter (Hastings model TNALL-50P) is read by a digital voltmeter whose output, in turn, was read during the experiment by the computer every 12 s. The flow was very stable and reproducible.

The approximately 4-MeV α particles from $^2H(t,\alpha)n$ leave the central target region through six tubes capped on their outer ends by 30-μg/cm^2, stretched polypropylene foils.[21] The reaction volumes are defined by 2-mm-wide, vertical slits in a stainless-steel ring positioned near the inner ends of the tubes and by 2-mm-diam apertures near the outer ends of the tubes. This arrangement defines six nominal reaction angles of 45°L, 45°R, 75°R, 90°L, 120°R, and 150°L (L and R indicate left and right of the incident beam as viewed in Fig. 2), gives a geometry factor[22] of about 40×10^{-5} cm sr at each angle, and has an angular acceptance in the reaction plane of 3.2° (FWHM) at each angle. Section III A includes a discussion of the determination of the true angles.

On emerging from the target and passing through the polypropylene foils, the reaction products impinge upon 50-μm-thick, silicon, surface-barrier detectors, and if they are energetic enough to pass through those detectors, they then enter similar detectors of 500-μm thickness. These detectors are mounted on a thermally insulated aluminum ring which is thermoelectrically cooled to about 0 °C. For the $^2H(t,\alpha)n$ experiment, only the 50-μm detectors were used, but during the $^2H(p,p)^2H$ calibration experiment described in Sec. III A, both the 50- and 500-μm detectors were used. The pulse-height information from these detectors is sent via standard NIM electronics to an on-line computer.

The energy widths of the α-particle peaks from $^2H(t,\alpha)n$ were about 45 keV and were determined mainly by detector and electronic noise, with the kinematic contribution being less than 15 keV.

C. Beam calorimeter

Because the low-energy beam undergoes significant charge exchange[23] in the target, we have chosen to determine the beam intensity by calorimetric means. The calorimeter is shown in Fig, 3, and its design is based on one from the University of Zürich.[24] A detailed description of our unit is given in Ref. 17. In brief, the collecting cup is biased cold by a thermoelectric cooling circuit and warmed back up to ambient temperature (thermistor no. 1 in Fig. 3) by power furnished by a heating transistor. Thus in the no-beam steady state, the heat furnished to the cup by the heating transistor is balanced by the constant heat withdrawn from the cup by the cooling circuit, and the cup is then at the same temperature as its surroundings, thereby reducing heat leaks. The heating-transistor power is measured accurately and regulated by an electronic circuit. When the beam is on, the power to the heating transitor is automatically decreased just

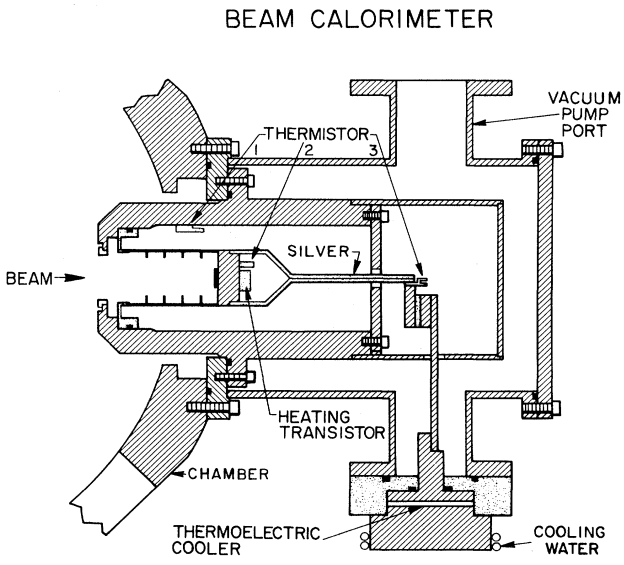

FIG. 3. Diagram of the calorimeter used to measure the low-energy beam intensity. The entrance aperture is 2.5 cm in diameter. The silver bands and plastic parts are shown stippled. The cross-hatched parts are copper except for the chamber (aluminum) and the outer vacuum case (brass). The beam collecting cup is electrically isolated, allowing the total beam charge also to be measured if desired.

enough to again bring the cup to ambient temperature. Thus, the decrease in power to the heating transistor is a measure of the beam power. The calorimeter control electronics measures the heating transistor power and generates an output pulse train whose frequency is proportional to the power. Thus, by scaling these output pulses the beam power is integrated over the run duration to yield the total energy furnished by the beam, independent of the beam's charge state. Knowledge of the beam energy per particle as it enters the calorimeter then allows us to calculate the beam flux. The beam-collecting cup is also electrically isolated to allow beam-current integration for tests and calibrations, and an electron suppressor ring is installed at the calorimeter entrance.

We calibrated the calorimeter with two methods: (1) a comparison with the integrated current of 10- and 3-MeV beams from the tandem Van de Graaff, and (2) using the known heat generated when an electrical current was passed through a precision, ($\pm 0.005\%$) 5-kΩ resistor (temperature coefficient of one part per million) embedded in the cup. Both methods agreed and resulted in a calibration constant of 97.80 ± 0.08 μJ per output pulse over a power range of 10—800 mW.

III. EXPERIMENT

A. Target density calibration with p + d elastic scattering

In order to measure absolute cross sections with the LEFCS target system, it is necesary to know the product of G, the geometry factor,[22] and n, the number of deuterium atoms per cm^3. Although G can be determined from the dimensions and locations of the detector collimators, and we did so determine G to about 1%, the quantity n is very difficult to calculate accurately from the two basic target parameters, flow rate and temperature, because of the nonstatic nature of the target. Therefore we chose to measure Gn by using p + d elastic scattering at an energy where the cross section is well known. Based on the reported p + d measurements of Ref. 25, we chose to calibrate at a bombarding energy of 10.04 MeV. Subsequently, however, it became clear that we needed to check the data of Ref. 25 and to improve their accuracy. We therefore used the tandem Van de Graaff accelerator and 30-inch precision scattering chamber[26] at the Los Alamos Ion Beam Facility to measure the differential cross section for p + d elastic scattering at 10.04 MeV proton bombarding energy.

Rather than measuring the individual parameters necessary to determine the cross section, we obtained a single overall normalization constant by bombarding a hydrogen target with 9.918-MeV protons and using the known p + p differential cross section that had been measured previously[26] to 0.5%. This calibration, along with the usual care taken[26,27] in measuring accurate absolute cross sections, allowed us to measure the p + d elastic differential cross section to 0.8% at laboratory angles of 45°, 75°, 90°, 120°, and 150°, and to 1% at 30°. The results are given in Table I. In Fig. 4 we compare the present measurements with those of Refs. 25 and 28, indicating our disagreement with the midangle data of Ref. 25.

TABLE I. Laboratory differential cross sections for p + d elastic scattering at a proton bombarding energy of 10.04 MeV. The 30° angle is accurate to 0.06° and the others are accurate to 0.03°.

θ_{lab} (deg)	σ_{lab} (mb/sr)	Relative error (%)	Total error (%)
30	239.36	0.42	0.96
45	144.35	0.44	0.79
75	31.11	0.44	0.79
90	15.82	0.42	0.78
120	26.02	0.43	0.79
150	41.93	0.42	0.78

The cross sections of Table I were then used in elastic p + d calibrations of Gn for the LEFCS cryogenic target. Two separate calibrations, which agreed with each other, were carried out separated by a time period of 10 months. To perform these calibrations a 10.04-MeV proton beam from the tandem Van de Graaff accelerator was directed into the LEFCS target (Fig. 2) through which $^2H_2$ gas was

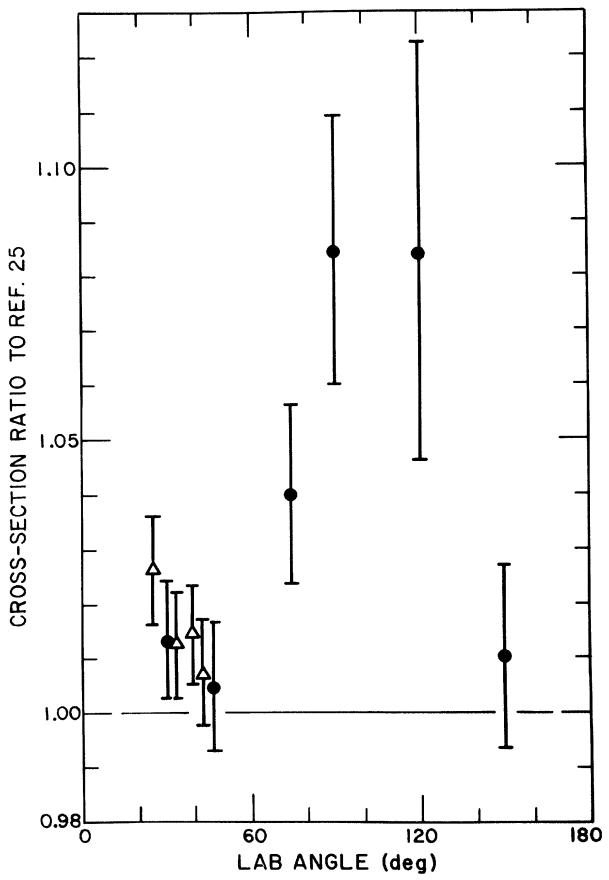

FIG. 4. Comparison of $^2H(p,p)^2H$ cross sections at 10.04-MeV proton bombarding energy. Data are shown as a ratio to the data of Ref. 25. The solid circles show the present data, and the triangles show the data of Ref. 28. Where the indicated errors significantly exceed 1%, they are due mainly to the data of Ref. 25.

flowing. In these measurements a standard Faraday cup was used in place of the calorimeter. The elastically scattered protons were detected at the six fixed angles given in Table II, which had been carefully measured with a telescope and dividing head to an accuracy of 0.03°. However, during an experiment the uncertainty in the actual beam direction raises the uncertainty in the laboratory angles to about 0.1°. Measurements were taken with gas flow rates F in the range 4—6 std cm^3/min and cooling-container temperatures T in the range 9.5—11.5 K, thus encompassing the nominal operating point of $F=5$ std cm^3/min and $T=10.5$ K. Before extracting Gn from these measurements, small corrections were applied to the cross sections of Table I because of the angle differences between Tables I and II. The angular shape of the cross section as given in Ref. 25, properly scaled according to Fig. 4, aided in making these corrections.

We were then able to extract from the p + d data the dependence of Gn on F and T and to study Gn, corrected to the nominal F and T, as a function of angle. We found that Gn was essentially independent of angle. Since we had designed and measured G to be independent of angle, this implies that the target density n does not depend on the angle at which the detector views the gas. This contradicts an earlier supposition we had entertained that at the highest and lowest angles n might be lower than at the central angles, because the detectors at the extreme angles observe a target region closer to the beam ports where the target gas flows out. Therefore, it is possible to give an angle-independent value of Gn for $^2H_2$ flowing through the LEFCS target:

$$Gn = 58.28 + 8.06(F-5) - 1.67(T-10.5)\,, \qquad (1)$$

where F is in std cm^3/min, T is in K, and Gn is in 10^{11} cm^{-2} sr. The standard deviation in Gn was determined to be 1.2%. We should point out that, because of the calibration method, it is the reproducibility of the measurements of F and T that is relevant and not their absolute accuracy. In addition, it might be thought that corrections would need to be made for the presence of impurities in the $^2H_2$ gas affecting the flow rate and possibly the measured yield. However, because the same bottle of gas was used during the calibration runs as was used during the entire ^{2}H(t,α)n experiment, no flow-rate corrections are necessary. Furthermore, the only significant impurity is H_2 (present at the 1% level); there is very little helium present and other impurities are frozen out before reaching the active target volume. In the low energy experiment, triton reactions on hydrogen are energetically forbidden, and in the calibration experiments proton scattering by hydrogen was kinematically separated in energy from scattering by deuterium. Therefore, no yield corrections are necessary either.

Estimates of the effect of local beam heating on the target density were made for both the calibration and the low-energy experiments. Even neglecting heat transfer by convection, the effect was found to be negligible. In addition, a low-energy experiment was carried out at 117 keV to a level of accuracy of 2%. No effect on the yield was seen when the beam intensity was changed by a factor of 2.5.

TABLE II. Detector angles for the LEFCS cryogenic target. L and R indicate left and right of the incident beam as viewed in Fig. 2.

Nominal angle	Actual angle
45°L	44.58°
45°R	45.44°
75°R	75.44°
90°L	89.56°
120°R	119.92°
150°L	149.52°

B. ^{2}H(t,α)n reaction

The procedure for carrying out the ^{2}H(t,α)n experimental runs began several days ahead of the start of actual data taking. During this period the system components, especially the flow apparatus and calorimeter, were checked for reliability and stability, the scattering chamber was pumped to about 2×10^{-7} Torr, and the liquid-nitrogen dewar was filled. On data-taking day the liquid-helium dewar was filled and the target was allowed to come to thermal equilibrium ($\frac{1}{2}$ to 1 h). With no target gas flowing, the $^3H^-$ beam was steered and focused through the target and into the calorimeter. By measuring the electrical current to both the target and calorimeter, the transmission through the target can be maximized. Generally, less than 0.5% of the beam actually hits the target beam ports. Furthermore, the target design is such that the majority of this beam strikes the target structure *before* entering the reaction volume, thereby minimizing errors in the beam intensity measurement. To further reduce this error (to a negligible level), the final beam-tuning adjustment is to weaken slightly the focusing of the einzel lens closest to the chamber. This has the effect of moving the beam waist toward the beam exit port, causing a small increase in the beam that hits the entrance port, but a decrease in that which hits the exit port. In addition, calculations of the increased beam divergence through multiple scattering when the target gas is introduced indicate a negligible decrease in the beam transmission.

The $^2H_2$ gas is then allowed to flow into the target, and the flow rate and target temperature are stabilized in preparation for data acquisition. The charge exchange in the beam caused by the target gas does not allow a continuous monitoring of possible small shifts in beam transmission; instead, during a series of runs, the gas flow is stopped occasionally, and the beam transmission is checked. Only very rarely did we find sufficient beam instability to warrant the discarding of data. During a run, the currents to the target and to the calorimeter and a chart recorder trace proportional to the calorimeter power level allow us to remain cognizant of any problems that might develop with the stability of the ion source. To initiate data taking, the beam is first intercepted just after passing through the bending magnet (Fig. 1), and the beam-off power level of the calorimeter is measured. The beam is then allowed to pass through the target, and a

data run of 10- to 90-min duration is carried out, depending on the counting rate. At the end of the run, the beam-off power level of the calorimeter is again determined. Rarely do the two beam-off measurements differ by more than 0.25%, and the average of the two is taken as the calorimeter baseline level for the run.

Every 24 h the 4-K pumping surfaces were warmed, the accumulated $^2H_2$ pumped away, and the liquid-He dewar refilled. Data were obtained at 17 triton bombarding energies from 12.5 to 117 keV, and at least two data runs were made, not always contiguously, at each energy. At the lowest energy, ten runs were made resulting in an accumulated beam flux of 60 particle mC. Throughout the course of data taking we employed beam currents from 1.4 to 4 μA and beam powers from 20 to 320 mW. The data were recorded and important parameters were monitored with the aid of the MODCOMP IV/25 on-line computer system and data-acquisition program Z at the Los Alamos Ion Beam Facility. In particular, the target temperature and $^2H_2$ flow rate were read and recorded every 12 s by the computer.

Figure 5 shows representative examples of the α-particle spectra. Except for a few low-channel counts at the highest energies, all the background is associated with the target gas being struck by the beam and is presumably due to $^2H(t,n)$ neutrons. Even at the lowest energy, $E_t = 12.5$ keV, the background was not a problem. We were limited at low energies by both the rapidly diminishing count rate and by the decreasing accuracy of the calorimeter at low power levels. The limit at high energy was voltage breakdown above 117 keV.

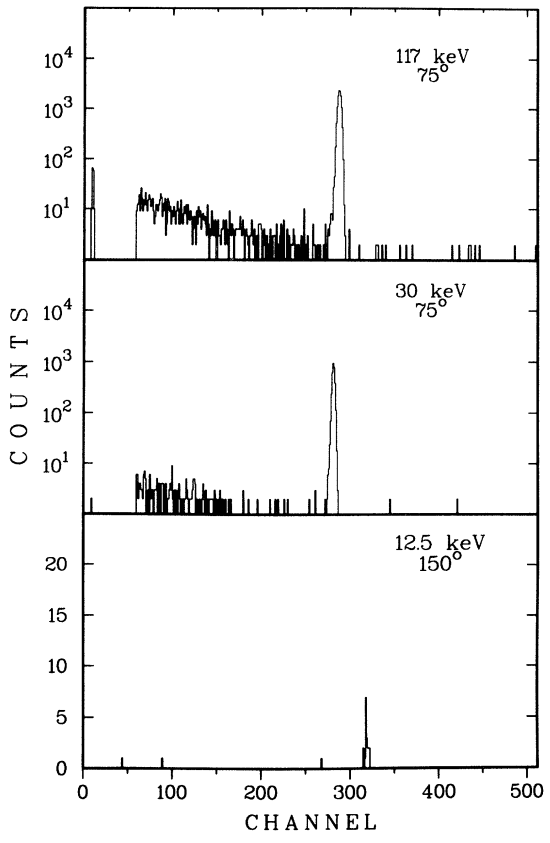

FIG. 5. Representative α-particle spectra from the $^2H(t,\alpha)n$ reaction at triton bombarding energies of 12.5, 30, and 117 keV produced with running times of 64, 86, and 13 min and containing 19, 3188, and 11 510 counts in the peaks, respectively.

IV. RESULTS

A. Data reduction and errors

Discussion of the data reduction and errors is best presented in reference to the formula for the laboratory differential cross section $\sigma_{lab}(\theta_{lab})$ at each bombarding energy:

$$\sigma_{lab}(\theta_{lab}) = 1.6022 \frac{N \sin\theta_{lab}}{QGn} \text{ (mb/sr)} . \quad (2)$$

In Eq. (2), N is the dead-time-corrected number of detected particles at laboratory angle θ_{lab}, Q is the integrated beam flux in particle mC, and Gn is in 10^{11} cm^{-2}sr and was discussed in Sec. III A.

In the discussion to follow it will be seen that there are some quantities whose uncertainties contribute in a correlated way to more than one factor in Eq. (2). In computing the final error in the cross section, such correlations have been treated properly. The errors (standard deviations) have also been separated into relative errors (Table III) and scale errors (Table IV), both with respect to bombarding energy. Relative errors fluctuate randomly from energy to energy, whereas scale errors are correlated from energy to energy such that if one happened to know how to correct such an error at one energy, then one could calculate the correction at the other energies as well. These scale errors generally are energy dependent; however, the overall scale error, as compounded quadratically at each energy from the individual contributions, does not vary greatly from energy to energy. Therefore, the energy-averaged value of 1.26% (Table IV) was adopted as a constant scale error to be added in quadrature to the (variable) relative error to obtain the total error in the cross section at each energy.

1. Bombarding energy

The beam energies at two locations are needed in the analysis: the triton energy E_t (or the equivalent deuteron bombarding energy E_d) at which the reaction takes place in the central region of the target and the energy E_c of the triton as it enters the calorimeter. E_t and E_c differ by the additional energy loss in the $^2H_2$ gas as the beam emerges from the target. The stopping powers of Andersen and Ziegler[29] were used to compute the energy losses in the target gas. For E_t these losses range from 36 eV at 12.5 keV to 93 eV at 117 keV, and for E_c the losses are twice those for E_t. We assign a relative error of 3% in the stopping power and a scale error of 8—12%, with the higher errors occurring at the lower energies. Further errors in the calculated energy losses arise from several effects: (a) 0.3% from the uncertainties in target gas flow rate and temperature, which affect the $^2H_2$ density; (b) a 10% uncertainty in the beam path length through the tar-

TABLE III. Contributions to the relative errors in the integrated cross section σ for the $^2H(t,\alpha)n$ reaction. For all items except the electronic dead time the larger errors occur at the lower bombarding energies.

Item	% error in σ
Counting statistics and background subtraction	0.3—4.6
Net calorimeter counts	0.1—0.8
Target density (flow and temperature stability)	0.3
Electronic dead time	0—0.1
Energy slope ($d\sigma/dE_t$)	0.01—0.08
Target stopping power	0.01—0.02
Accelerator voltage instability	0—0.01

get gas; and (c) 2% from the determination of n through the individual measurements of Gn and G.

The beam accelerating voltage is known from the calibration of the resistive divider and associated digital voltmeter, which was carried out to an accuracy of 0.008% at the Sandia National Laboratories Primary Standards Laboratory. This calibration was rechecked 21 months after the initial calibration, and the long term stability of the divider was found to be excellent. Beam energy instabilities during the individual runs were determined from observation of the divider digital voltmeter to be quite small, 1—4 eV, with the higher values occurring at the higher energies.

A small correction to the beam energy arises from plasma conditions in the duoplasmatron ion source. The $^3H^-$ ions are preaccelerated through the anode hole by a fraction of the arc voltage. This correction must be significantly less than the voltage between the intermediate electrode and the anode hole, which we measured to be 35 V. We used information from Ref. 30 to obtain an estimate for this correction, and have added 5 ± 3 eV to the beam energy. The energy results are given in Table V.

Errors in the beam energies affect the measured cross sections σ in two ways: (1) through the determination of the beam flux Q as discussed in Sec. IV A2, and (2) through the energy slope $d\sigma/dE_t$ of the cross section. This latter contribution to the error in σ is obtained by multiplying the slope by the standard deviation in E_t.

The beam-energy spread was studied by oscilloscope observation of rapid fluctuations in and ripple on the accelerating voltage; this results in spreads of 3—22 eV. Other contributions to the energy spread are the following: (a) 15 eV from source plasma conditions, (b) 8—22 eV from energy straggling in the target gas, and (c) 10—25 eV from the finite length of beam observed by the detectors. All these contributions increase with increasing beam energy. Compounding these contributions in quadrature gives an estimate of 20—43 eV for the beam-energy spread over the energy range of the present experiment. These spreads are sufficiently small that no corrections need to be applied to the measured cross sections.

We also considered the possibility that a "tandem accelerator" effect could occur in the 10- to 25-kV gridded einzel lens nearest to the scattering chamber. If the charge exchange $^3H^-$ to $^3H^+$ were to occur at appropriate locations in the region of the lens's electrostatic field, then an acceleration of the ion could occur up to twice the lens voltage. Although such ions would not be focused by the lens, some of these "hot" particles might find their way into the target region and would have a considerably

TABLE IV. Contributions to the scale error in the integrated cross section σ for the $^2H(t,\alpha)n$ reaction. For each item the larger errors occur at the lower bombarding energies.

Item	% error in σ
Gn calibration	1.2
Energy slope ($d\sigma/dE_t$)	0.02—0.32
Target transmission[a]	0.3[a]
Calorimeter calibration	0.08
Target stopping power	0.01—0.07
Beam path length through target gas	0.02—0.06
Detector angles	0.05
Source plasma preacceleration	0—0.02
Resistive divider and digital voltmeters	0.01
Target density	0—0.01
Beam heating	0
Finite geometry	0
Adopted scale error	1.26%

[a]Only applied before the final beam-tuning adjustment described in Sec. III B was adopted.

TABLE V. Energy relationships for ^{2}H(t,α)n. The energies are expressed in keV. E_0 is the nominal triton bombarding energy, E_t is the triton energy at the center of the gas target, E_c is the triton energy as it enters the beam calorimeter, and E_d is the deuteron bombarding energy that is equivalent to E_t. The total error in E_t is dominated by the scale error and varies from 6 eV at 12.5 keV to 16 eV at 117 keV, whereas the relative error varies from 1 to 5 eV. The errors for E_c are approximately twice those for E_t.

E_0	E_t	E_c	E_d
117	116.912	116.819	78.066
115	114.913	114.821	76.731
110	109.913	109.821	73.392
105	104.914	104.823	70.054
100	99.914	99.823	66.716
90	89.917	89.829	60.040
80	79.919	79.833	53.364
70	69.923	69.841	46.690
60	59.927	59.849	40.015
50	49.932	49.859	33.341
40	39.938	39.871	26.668
30	29.945	29.885	19.995
25	24.950	24.895	16.660
20	19.956	19.907	13.325
17.5	17.459	17.413	11.658
15	14.962	14.919	9.991
12.5	12.469	12.433	8.326

larger cross section for the ^{2}H(t,α)n reaction than do the "normal" particles. Principally for that reason we installed directly beneath the lens a cryopump that keeps the pressure in that region in the low 10^{-7} Torr range. A calculation indicates that at that pressure the charge-exchange effect in question is completely negligible. Furthermore, charge exchange in the lens grid occurs only in a very thin surface layer, and we calculate that this source of "hot" particles would also cause no problem. In addition, the kinematic separation in energy of the detected alpha particles from the two beam components would normally be readily observable at the forward and backward laboratory angles.

Finally, we should mention that in the initial development of the LEFCS facility an alternate method of measuring the beam energy was studied. In that method[31] we measured the flight time of a packet of neutral beam atoms produced by exposing the negative component in the beam to a fast pulse of 1-μm radiation from a Nd:YAG laser. Shifts in the beam energy of a few tens of eV were readily observed; however, we have not yet obtained sufficient stability and reproducibility to make accurate absolute energy measurements. For example, we have been able to check the triton beam energy to an accuracy of only 50 to 100 eV at 20 keV. Use of this method has been abandoned for the time being.

2. Beam flux

To determine the beam flux Q in Eq. (2) we use the relationship

$$Q = 0.0978 C_0 / E_c \text{ (particle mC)} , \tag{3}$$

where E_c is the beam energy in eV as it enters the calorimeter (Table V) and C_0 is the net number of output pulses from the calorimeter (see Sec. II C). C_0 is obtained from

$$C_0 = \nu_b t - C , \tag{4}$$

where t is the run time, ν_b is the calorimeter baseline frequency (about 9600 Hz) as determined from measurements immediately before and after each run, and C is the number of calorimeter output pulses during the run. The run time was generally measured to 0.1 s, and the error in ν_b depends on the change observed in the baseline frequency from the beginning to the end of the run and on uncertainties in the correction for drifts in room temperature. The resulting error in C_0 is about 0.1% at the higher energies, increasing to about 1% at the lower energies where the beam power is smaller. The errors in E_c and the numerical constant in Eq. (3) have already been discussed. The effect on Q of beam backscattering out of the calorimeter was calculated and found to be negligible.

We have also investigated, both with calculations and by experiment, whether or not anomalous particle paths caused by charge exchange in the beam line, say from negative to neutral species, could cause a problem with the yield determination. It is possible to conceive that such particles could enter the target reaction volume, but strike the beam exit port instead of entering the calorimeter. We conclude, however, that any such effect is at too low a level to influence our results.

3. Other quantities

Besides affecting the determinations of the energies E_t and E_c, the uncertainties of 0.02 std cm^3/min and 0.02 K

TABLE VI. Integrated cross section σ and astrophysical S function for the ^{2}H(t,α)n reaction. E_0 is the nominal triton bombarding energy. For the accurate energies see Table V. The total error is obtained by adding in quadrature a 1.26% scale error to the relative error.

E_0 (keV)	σ (mb)	S (MeV b)	Relative error (%)	Total error (%)
117	3739	26.64	0.52	1.36
115	3655	26.74	0.48	1.35
110	3352	26.30	0.54	1.37
105	3074	26.00	0.47	1.34
100	2752	25.28	0.56	1.38
90	2166	24.02	0.47	1.34
80	1590	22.19	0.50	1.36
70	1114	20.70	0.45	1.34
60	703.6	18.87	0.42	1.33
50	396.9	17.35	0.51	1.36
40	182.4	15.81	0.82	1.50
30	58.13	14.32	0.68	1.43
25	26.28	13.92	1.01	1.62
20	8.77	13.43	2.01	2.37
17.5	4.13	12.83	3.15	3.39
15	1.784	13.48	2.86	3.12
12.5	0.525	12.63	4.59	4.76

in the target gas flow rate and temperature, respectively, also contribute a 0.3% error in Gn through Eq. (1).

The uncertainty in the laboratory angles of about 0.1° causes an error in the laboratory differential cross section [Eq. (2)] through the sine factor and the dependence of the number of detected particles on laboratory angle. In addition, a further error is contributed through the Jacobian in converting to the c.m. system (Sec. IV A*4*). The overall effect is small and only results in a 0.05% contribution to the final error in the cross section.

The α-particle spectra were relatively free of background counts in the region of the peaks, and therefore, the error due to background determination is negligible. Counting statistics contribute errors of 0.3—0.4 % at the higher energies, increasing to 4.6% at the lowest energy. The counting rates were low enough that the dead-time corrections were 1% or smaller.

The sizes of the detector apertures were large enough that a small finite-geometry correction of about 0.2% was made to the ^{2}H(t,α)n cross sections. This correction arises because of the significant difference in the shape of the laboratory differential cross section for the p + d calibration data and for the ^{2}H(t,α)n measurements.

All the error contributions just discussed are summarized in Tables III and IV, where their effects on the error in the integrated cross section σ are presented.

4. *Integrated cross sections*

For each run the laboratory cross section was obtained from Eq. (2) and converted to the c.m. differential cross section. To within the relative error of 1% in the detection efficiencies of the six detectors, we obtained the expected[2,3,9] isotropy of the c.m. differential cross section. Therefore, the integrated cross section σ for each run was obtained by summing the six values for the c.m. differential cross section and then multiplying by $4\pi/6$. At each bombarding energy a weighted average of σ for each run was computed, where the weighting factor was the beam flux Q for that run. The values of σ so obtained are listed versus bombarding energy in Table VI and are plotted in Fig. 6. It is seen that the σ measurements cover a range of four orders of magnitude from 3.74 b down to 0.525 mb. This lowest value corresponds to a differential cross section of about 40 μb/sr, which is not extremely low; however, it must be remembered that we have used a very thin target, thereby sacrificing some counting rate in order to obtain accurate bombarding energies.

5. *Astrophysical S function*

For analyses and comparisons, the data presentation in Fig. 6 is not very useful, because of the highly compressed cross-section scale. A much better representation of the data for such purposes is in the form of the so-called astrophysical S function,[32–36] which is universally used in the field of nuclear astrophysics. The S function is useful for treating reactions at energies below the Coulomb barrier (440 keV for d + t) and is obtained by factoring out from the cross section the energy dependences of $\lambda\!\!\!^{-2}$ and the Coulomb penetrability in the incident channel. This procedure relegates to S an energy dependence more nearly representative of explicitly nuclear effects. For reactions having a d + t incident channel, S is given by

$$S=\sigma E\exp(1.08727E^{-1/2}),$$

or, equivalently,

$$S=0.40038\sigma E_t\exp(1.71830E_t^{-1/2}),$$

or, equivalently,

$$S=0.59962\sigma E_d\exp(1.40411E_d^{-1/2}), \quad (5)$$

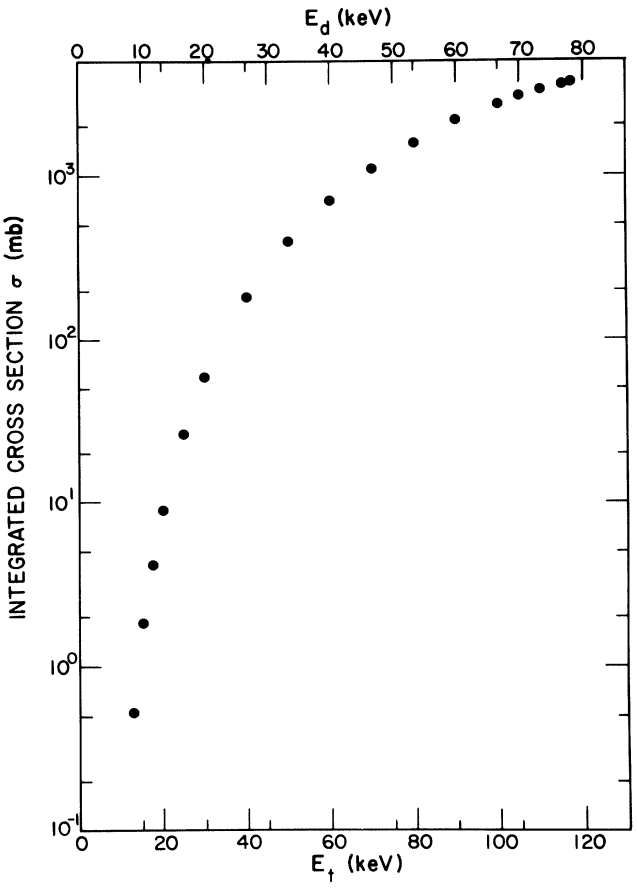

FIG. 6. Integrated cross section for the ^{2}H(t,α)n reaction versus triton (E_t) or equivalent deuteron (E_d) bombarding energy as measured in the present work. The unlabeled ticks on the cross-section scale have most significant digits of 2 and 5. The small unlabeled ticks on the energy scales match the labeled ticks on the opposite scale.

where σ is the cross section in b; E is the incident-channel c.m. energy in MeV; E_t and E_d are the triton and deuteron bombarding energies, respectively, in MeV; and S is expressed in units of MeV b. Values of S for the present data are listed in Table VI and are plotted in Fig. 7. As is done in Fig. 7, we generally will present our data as a function of equivalent deuteron bombarding energy in order to comply with the usual convention for this reaction.

B. Data comparisons

Figures 8—10 display the existing ^{2}H(t,α)n data in the form of S vs E_d for E_d below 140 keV. S displays the typical bell shape appropriate to a reaction that proceeds through a well-isolated nuclear level. It is seen that the present data are considerably more accurate than those of previous work, our errors being generally at least a factor of 3 smaller. Our results appear to be in reasonably good agreement with the data of Conner *et al.*[4] (Fig. 8) and Arnold *et al.*[6] (Fig. 10), although some systematic differences can be noted. The measurements of Bretscher and French[2] and of Jarvis and Roaf[5] (Fig. 10) are in marked disagreement with the present experiment, and although the data of Katsaurov[7] and Argo *et al.*[3] (Fig. 9) do not have a large overlap with our energy range, they do seem on the average to lie somewhat higher than our values. The data of Kobzev *et al.*[8] (Fig. 8) do not overlap in energy with ours, but do lie below the smooth trend indicated by our highest energy measurements.

We should mention here that in some earlier presentations of our ^{2}H(t,α)n measurements,[15,16] a possible unexpected structure of S in the low-energy region was suggested by the data. This impression arose because the two data points at triton energies of 15 and 20 keV fell more than one standard deviation above the smooth trend displayed by the remainder of the data. Although we calculated that, from purely statistical considerations, such a

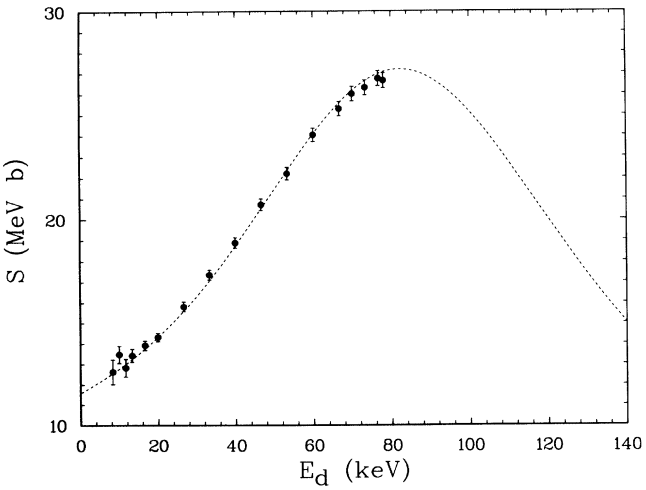

FIG. 7. The S function [Eq. (5)] vs equivalent deuteron bombarding energy E_d for the present ^{2}H(t,α)n experiment. Total errors are shown. Note the suppressed zero. The curve is the result of the single-level fit discussed in Sec. V A.

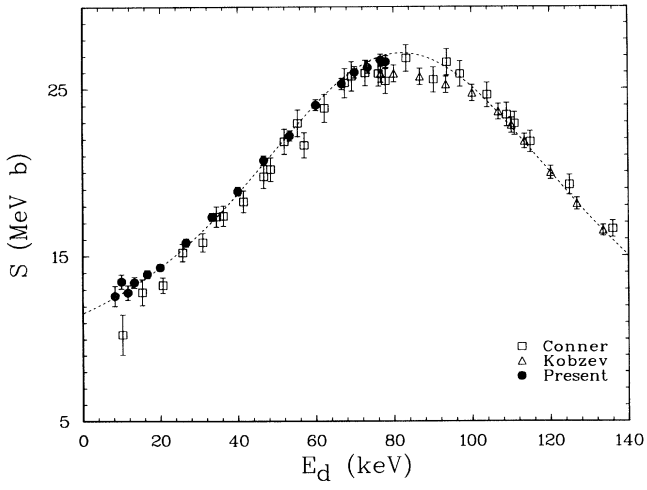

FIG. 8. The S function [Eq. (5)] vs equivalent deuteron bombarding energy E_d for the ^{2}H(t,α)n reaction. Shown are the present data and those of Refs. 4 and 8. Note the suppressed zero. Total errors are indicated. The curve is the result of the single-fit discussed in Sec. V A.

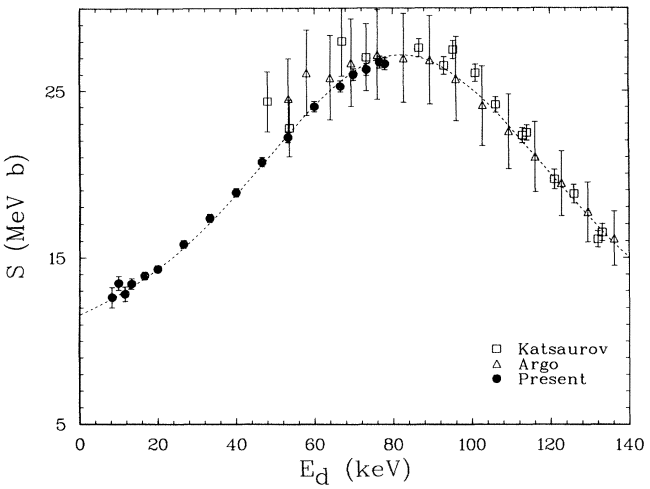

FIG. 9. The S function [Eq. (5)] vs equivalent deuteron bombarding energy E_d for the ^{2}H(t,α)n reaction. Shown are the present data and those of Refs. 3 and 7. Note the suppressed zero. Total errors are indicated. The curve is the result of the single-level fit discussed in Sec. V A.

structure could appear with a probability of 1 in 20, we deemed the question of possible structure in the low-energy region of the ^{2}H(t,α)n reaction to be of sufficient importance to obtain additional data. Therefore, we remeasured the cross section at triton energies of 15, 20, and 25 keV and measured an additional point at 17.5 keV. We took even more precautions with obtaining good target transmission during these repeat measurements, and in fact sacrificed some further beam intensity to that end. The results indicate that no structure is present; each new point falls within one standard deviation of the smooth curve shown in Fig. 4 of Ref. 16. Using standard statistical criteria, we have no reason to discard the earlier results,[15,16] and therefore those data were averaged with the more recent data to obtain the results presented here.

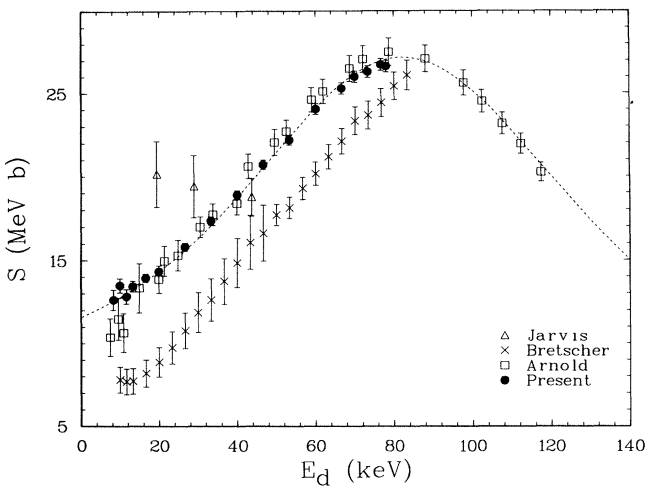

FIG. 10. The S function [Eq. (5)] vs equivalent deuteron bombarding energy E_d for the ^{2}H(t,α)n reaction. Shown are the present data, those of Refs. 2 and 5, and a portion of those of Ref. 6. Note the suppressed zero. Total errors are indicated. The curve is the result of the single-level fit discussed in Sec. V A.

V. CALCULATIONS

A. Single-level fit

R-matrix theory[37] has been extremely useful in describing reactions among light nuclei and has, in particular, been used to help understand reactions important to fusion energy.[9] Although a current R-matrix analysis of the mass-5 system[9] has covered the energy range up to about 10 MeV deuteron bombarding energy and has used a multilevel approach, it might be expected that a single-level approach would be valid up to a few hundred keV because of the dominance of the $\frac{3}{2}^+$ resonance in this energy region. Therefore, we have constructed a data base for deuteron energies up to about 250 keV, using our data and those of Refs. 4 and 6–8, and have performed a single-level fit to this data base in the R-matrix formalism. For such a fit the theoretical cross section is given by[37]

$$\sigma=\pi\lambda\!\!\!^{-2}g\Gamma_d\Gamma_\alpha/[(E_\lambda+\Delta_\lambda-E)^2+\Gamma_\lambda^2/4]\ , \tag{6}$$

where $\lambda\!\!\!^{-}$ is the reduced deBroglie wavelength in the incident channel; g is a statistical weight that here is equal to $\frac{2}{3}$; the subscripts d and α refer, respectively, to the incident d + t and exit α + n channels; E_λ is the level energy; the Γ are the partial and total widths; Δ_λ is the level shift; and E is the c.m. energy. The partial widths Γ_c (with c equal to d or α) are expressed in terms of the penetrabilities P_c and reduced widths γ_c through the relation

$$\Gamma_c=2P_c\gamma_c^2\ , \tag{7}$$

and the total width Γ_λ is given by

$$\Gamma_\lambda=\Sigma\Gamma_c=\Gamma_d+\Gamma_\alpha\ . \tag{8}$$

The usual level subscript (λ) is omitted from some quantities because only one level is involved here. Part of the energy dependence of σ occurs through the penetrabilities, which are defined in terms of the fixed channel radii a_c, the wave number $k=\lambda\!\!\!^{-1}$, and the Coulomb functions F_l and G_l evaluated at a_c:

$$P_c=ka_c/(F_l^2+G_l^2)\ . \tag{9}$$

In Eq. (9) l refers to the relative orbital angular momenta, which here are $l=0$ for the d channel and $l=2$ for the α channel. These are the lowest values consistent with the reaction's proceeding through a $\frac{3}{2}^+$ level. Although $l=2$ is also allowed in the incident channel, the high angular momentum barrier at the low bombarding energies under consideration makes its contribution to the cross section negligible.

The level shift Δ_λ in Eq. (6) is the sum over the partial level shifts Δ_c:

TABLE VII. Parameters for the single-level fit discussed in Sec. V A. E_λ is channel independent. The quoted errors neglect correlations and are computed from the diagonal elements of the covariance matrix of Table VIII.

Channel	a_c (fm)	B_c	l	γ_c (MeV$^{1/2}$)	E_λ (MeV)
d + t	5.00	−0.27864	0	4.6059±1.5245	0.05057±0.00778
α + n	3.00	−0.557	2	1.0006±0.3250	0.05057±0.00778

$$\Delta_\lambda = \Sigma\Delta_c = \Delta_d + \Delta_\alpha \,, \tag{10}$$

with

$$\Delta_c = -\gamma_c^2 (S_c - B_c) \,. \tag{11}$$

Here B_c is a fixed boundary-condition parameter, and the shift function S_c is a function of energy through its dependence on the Coulomb functions and their derivatives, all evaluated at a_c:

$$S_c = P_c (F_l F_l' + G_l G_l') \,. \tag{12}$$

The main energy dependence in Eq. (6) is through Γ_d, which contains the Coulomb penetrability in the incident channel. Equation (5) essentially factors out this dependence from σ through an accurate approximation[32,38] for the Coulomb functions at low energies. The remaining energy dependences in Eq. (6) are thus relegated to the astrophysical S function of Eq. (5).

All the parameters for the fit are given in Table VII. The channel radii a_c are chosen to divide configuration space into an internal region, where the nuclear force dominates the interaction, and an external region, where at most a Coulomb force is present. Other than that, there is considerable freedom in their choice; we chose the same values used in the multilevel analysis of Ref. 9. There are several reasonable procedures[37,39] for selecting the boundary-condition parameters B_c. Here we chose B_c so that the level shifts Δ_c are zero near the peak of the S function, which results in the level energy E_λ being close to the c.m. energy at which the S function peaks. However, this is not at all necessary, because the simple structure of the single-level approximation results in identical fits for any values of B_c—E_λ will simply change to compensate for changes in B_c. With a_c and B_c fixed, there are three remaining parameters to be varied in the fit, E_λ (in actual fact $\sqrt{E_\lambda}$ is used in the computer code), γ_d, and γ_α. The resulting values for these parameters are also given in Table VII. A good fit to the above-mentioned data base was achieved with a χ^2 per datum of 1.33 for 177 data points. Both the fit and the data base are presented in Fig. 11 as integrated cross section versus deuteron bombarding energy. This fit is also shown as dashed curves in Figs. 7—10. Thus we see that the variation with energy of the cross section is well reproduced theoretically through the energy dependences both of the R matrix, which furnishes the c.m. energy E in the denominator of Eq. (6), and of the Coulomb functions as expressed in the penetrabilities and level shifts. A Lorentzian function of energy fits S moderately well in the resonance region, but not nearly so well as does the full R-matrix formalism, especially on the low-energy side of the resonance.

The covariance matrix,[40] sometimes called the error matrix,[41] for the fit is listed in Table VIII. This matrix is given by twice the inverse of the matrix of second derivatives of χ^2 with respect to the fitting parameters $\sqrt{E_\lambda}$, γ_d, and γ_α, the derivatives being evaluated at the minimum of χ^2. It is usual to quote as the error in a fit parameter the square root of the associated diagonal element of the covariance matrix; however, giving only this error does not allow the correlations in the parameters to be taken into account. This simplified error is quoted in Table VII. When the full covariance matrix is used to compute the error in the fitted S function (or in σ) the result is as follows: At the very low energies the error is about 0.5%, drops gradually to about 0.3% as the energy E_d increases to near 125 keV, and rises again to about 0.5% as E_d increases to 250 keV. Our best determination of S_0, the S function evaluated at zero energy, is $S_0 = 11.59 \pm 0.06$.

On comparing the present single-level parameters with those of the appropriate level from the multilevel fit of Ref. 9, we find the latter reduced widths to be several

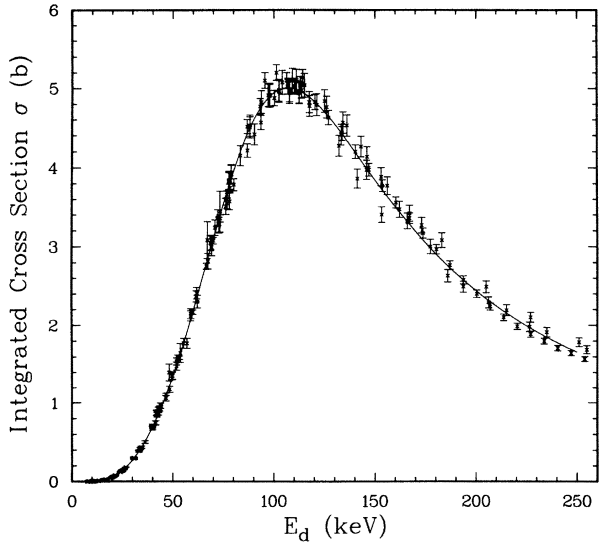

FIG. 11. Integrated cross section σ for the ^{2}H(t,α)n reaction versus equivalent deuteron bombarding energy E_d. The curve is from the single-level fit discussed in Sec. V A, and the points represent the data base used to generate that fit.

TABLE VIII. Elements of the symmetric covariance matrix for the single-level fit discussed in Sec. V A. The elements have units of MeV$^{1/2}$ and are indexed as follows: $1=\sqrt{E_\lambda}$, $2=\gamma_d$, and $3=\gamma_\alpha$. The numbers in parentheses give the power of 10 by which the preceding number is to be multiplied.

	1	2	3
1	0.29893(−3)		
2	0.31104(−3)	2.3241	
3	0.10933(−3)	0.49544	0.10563

times smaller than the present ones. However, it is not possible to draw any simple conclusions from this fact, because as pointed out by Hale,[42] one must really compare the structure (poles and residues) of an asymptotic quantity, such as the S matrix. This would involve[42] the use of Coulomb functions of complex arguments, and though such a comparison would be very interesting to make, the necessary effort to do this accurately for ^{2}H(t,α)n near threshold has not yet been expended. In the energy range of our data, the fit of Ref. 9 gives cross-section predictions that are about 7% below our measurements. A reanalysis is underway in which the present data are included.

We have fitted a polynomial in E to the low energy ($E_d<78$ keV) portion of the S function obtained from the single-level fit, and these results are given in Table IX. Thus the use of Table IX and Eq. (5) allows one to obtain rather simply our best determination of the cross section for the ^{2}H(t,α)n reaction on the low-energy side of the $\frac{3}{2}^+$ resonance.

B. Reactivity

In a d + t plasma in thermal equilibrium at temperature T, the ^{2}H(t,α)n reaction rate is calculated by multiplying the product $n_d n_t$ of the number densities of deuteron and triton nuclei by the reactivity $\langle\sigma v\rangle$. This reactivity[32–36] is the product of the reaction cross section σ times the relative velocity v of the reacting nuclei averaged over the Maxwell-Boltzmann velocity distribution appropriate to the plasma temperature. If the cross section is written in terms of an S function as in Eq. (5), then when S has a simple energy dependence, the integral for $\langle\sigma v\rangle$ can be evaluated[34,36] quite accurately by a corrected version of the steepest descent method. When S has an energy dependence complicated enough that it is preferable to evaluate $\langle\sigma v\rangle$ numerically, it can still be useful to employ an analytical evaluation of the integral by introducing an effective, Maxwell-Boltzmann averaged S function, $\langle S\rangle$, and evaluating the integral with S set to unity. This then serves as a definition of $\langle S\rangle$, and for a d + t plasma we may write

$$\langle\sigma v\rangle=5.967\times10^{-16}\langle S\rangle\tau^2e^{-\tau}[1+5/(12\tau)]\ , \quad (13)$$

with

$$\tau=19.983/(kT)^{1/3}\ . \quad (14)$$

Here k is Boltzmann's constant, and kT is in keV, $\langle\sigma v\rangle$ is in cm^3/s, and $\langle S\rangle$, which is a function of kT, is expressed in MeV b. Generally, $\langle S\rangle$ is a very useful form in which to present and compare reactivities, because it will normally have a much weaker temperature dependence than does $\langle\sigma v\rangle$. Thus the function $\langle S\rangle$ bears a relationship to $\langle\sigma v\rangle$ similar to that of the S function to σ. For example, if S had the value S_0 independent of energy, then $\langle S\rangle$ would be independent of kT and in fact would equal S_0. The extent to which $\langle S\rangle$ varies with kT reflects the extent to which S varies with E. Because of our desire to stress that relationship between S and $\langle S\rangle$, we chose to incorporate the factor $1+5/(12\tau)$, which arises from a first order correction to the reactivity integral, explicitly into Eq. (13) rather than to include it implicitly in $\langle S\rangle$. This is not in accord with the usual convention in nuclear astrophysics[32–36] in which the effective S function $S_{\rm eff}$ is related to our $\langle S\rangle$ by $S_{\rm eff}=\langle S\rangle[1+5/(12\tau)]$.

In the present work, where S has a resonant structure, we evaluate $\langle\sigma v\rangle$ numerically using Eq. (4-44) of Ref. 35 and convert it to $\langle S\rangle$ through Eq. (13). In this procedure we use the cross section obtained from our single level fit (Sec. V A). Because that fit yields S only up to a deuteron energy of about 250 keV, it turns out that the calculation of $\langle\sigma v\rangle$ and $\langle S\rangle$ begins to lose accuracy above a plasma temperature kT of about 20 keV. Therefore, we present reactivities only for $kT=0$–20 keV. A small correction was applied near 20 keV by making a reasonable extrapolation of σ to energies above $E_d=250$ keV.

The result we obtain for $\langle S\rangle$ is shown as a solid curve in Fig. 12. There we also compare our determination of the ^{2}H(t,α)n reactivity with other work.[10–13] Greene[10] used cross sections published through 1964 and fitted logσ vs log$E$ to polynomial functions which were then incorporated into the reactivity calculation. It is seen in

TABLE IX. Coefficients e_n of a polynomial fit in c.m. energy E to the low-energy portion of the S function obtained from the single-level fit described in Sec. V A. The series for S is a sum of terms of the form e_nE^n for $n=0$ to 4. To convert to a series in triton bombarding energy E_t, multiply e_n by $(0.40038)^n$. To convert to a series in deuteron bombarding energy E_d, multiply e_n by $(0.59962)^n$. The fit is valid for E, E_d, and E_t less than 46.8, 78, and 117 keV, respectively. The maximum error in reproducing the single-level S function in this energy range is 0.06%, which occurs at the end points of the energy range. The units of e_n are such that S is in MeV b when the energies are in keV. The numbers in parentheses give the power of 10 by which the preceding number is to be multiplied.

n:	0	1	2	3	4
e_n:	11.586	0.18478	0.92092(−3)	0.27462(−3)	−0.48693(−5)

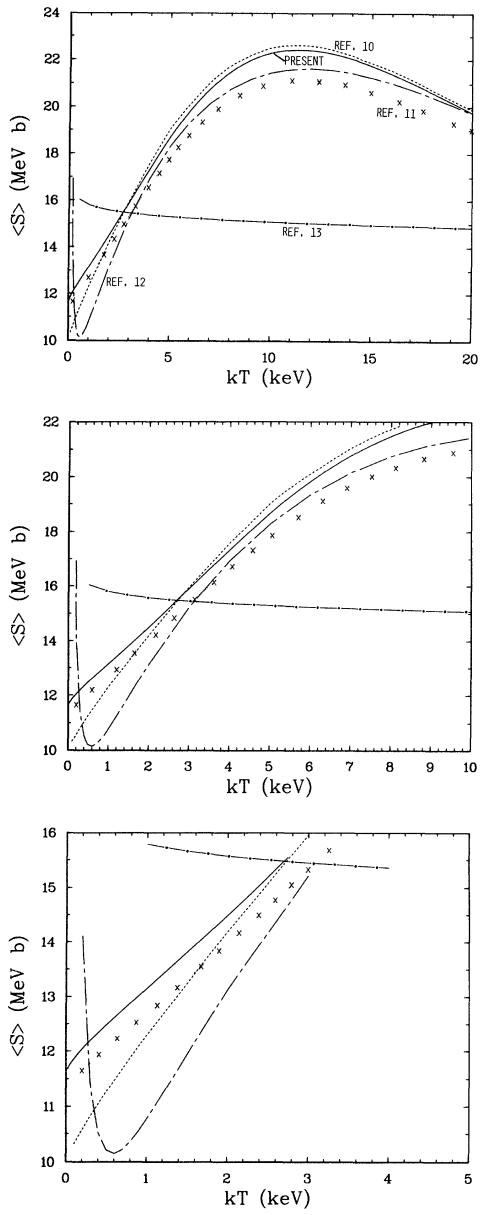

FIG. 12. Maxwell-Boltzmann averaged S function, $\langle S \rangle$, from which the ^{2}H(t,α)n reactivity $\langle \sigma v \rangle$ can be calculated using Eqs. (13) and (14). kT is the plasma temperature in keV. Two graphs having expanded scales are also shown. The solid curve represents the present work, the dashed curve is from Greene (Ref. 10), the crossed curve is from Hale (Ref. 11), the chain-dashed curve is from Hively (Ref. 12), and the chain-dotted curve is from Glasstone and Lovberg (Ref. 13).

Fig. 12 that above temperatures of a few keV we are in excellent agreement with Greene, but at the very low temperatures we obtain significantly higher reactivities, with the disagreement approaching 20% at zero temperature. Hively[12] made an accurate fit [his functional form S_5 of Eq. (5) and Table I of Ref. 12] to the reactivities of Miley *et al.*,[43] who in turn had used the cross-section fits of Duane.[44] We are in moderate disagreement with Hively over the entire temperature range, and, in addition, it seems that the functional form adopted by Hively introduces a pathological behavior at very low temperatures, which is an example of what can occur with a fitting function that has very little physical foundation. Hale[11] used the cross-section results of the multilevel fit of Ref. 9 to compute ^{2}H(t,α)n reactivities. It is seen that we obtain larger reactivities than does Hale, with significant disagreement at the higher temperatures; however, we do agree best with Hale at the lower temperatures. Glasstone and Lovberg[13] present a formula which admittedly does not contain the proper resonant structure for the ^{2}H(t,α)n reaction. Nevertheless, they do imply the validity of the formula at low temperatures. However, Fig. 12 illustrates quite strikingly that that formula,[13] and in fact all formulas of a nonresonant type, should be avoided when dealing with ^{2}H(t,α)n reactivities in this temperature region.

In Table X we present the results of a polynomial fit to the quantity $\langle S \rangle$ of the present work. We take $z=(kT)^{1/3}$ as the indepenent variable, because such a form for S_{eff}, and hence for $\langle S \rangle$, follows from the mathematics of the reactivity integral.[33,34] The use of this form, as opposed to the use of a polynomial in kT, ensures especially that the low-temperature behavior of $\langle S \rangle$ is properly reproduced; in particular that $\langle S \rangle$ should intercept the $kT=0$ axis with infinite slope. Table X combined with Eqs. (13) and (14) presents the reactivity $\langle \sigma v \rangle$ in a form suitable for easy computation.

VI. CONCLUSIONS

We have developed and installed at the Los Alamos Ion Beam Facility an apparatus, the low-energy fusion cross-section (LEFCS) system, for making highly accurate measurements of cross sections for nuclear reactions of importance for fusion energy production, and we have presented here the results of our first study with the LEFCS system, measurements of the cross section for the ^{2}H(t,α)n reac-

TABLE X. Coefficients t_n of a fit in plasma temperature kT to the Maxwell-Boltzmann averaged S function, $\langle S \rangle$, discussed in Sec. V B and presented as a solid curve in Fig. 12. The polynomial fit for $\langle S \rangle$ is a sum of terms of the form $t_n z^n$ for $n=0$ to 11, with $z=(kT)^{1/3}$. The series is valid for kT from 0 to 20 keV with a maximum error in reproducing $\langle S \rangle$ of 0.04%. The units of t_n are such that $\langle S \rangle$ is in MeV b when kT is in keV.

n:	0	1	2	3	4	5
t_n:	11.592	1.7147	−19.241	101.38	−276.41	462.39
n:	6	7	8	9	10	11
t_n:	−495.80	346.21	−155.60	43.179	−6.7126	0.44667

tion. The present data are by far the most accurate ever obtained for this reaction over the low-energy side of the $\frac{3}{2}^+$ resonance. We combined our data with several other sets covering the resonance region (E_d=0–250 keV) and performed a single-level fit to the cross section. The result of this fit yields a highly reliable representation of the ^{2}H(t,α)n cross section that is suitable for use in fusion-energy calculations in this energy region. We used this fit to calculate ^{2}H(t,α)n reactivities for plasma temperatures up to 20 keV. Comparison with previous calculations shows that our reactivities best agree with Greene[10] at the higher temperatures, but best agree with Hale[11] at the lower temperatures. Of course a good multilevel fit to ^{2}H(t,α)n over a broad energy range, along the lines described in Ref. 9, will be of great value. Such a fit could possibly yield slight improvements in the low-energy region, but more importantly, would allow reactivity calculations at higher plasma temperatures.

We should remind the reader that for very low energy nuclear reactions it is sometimes important to take account of the shielding[6,35,45] of the nuclei by electrons in the reaction environment, such as in a standard cross section measurement or in a hot plasma. Such shielding can result in an increase in the effective reaction energy (or equivalently a lowering of the Coulomb barrier) with respect to interacting bare nuclei, with a consequent increase in the nuclear reaction rate. For example, if a deuteron (^{2}H$^+$ ion) were incident on a neutral tritium atom and if the electron motion were not perturbed significantly by the incident deuteron, then the energy of the deuteron at the tritium nucleus would be increased by e^2/a_0=27 eV, where a_0 is the Bohr radius. If the deuteron laboratory energy were 10 keV, this atomic shielding would cause an increase of 2.7% in the reaction rate. Thus it is possible that at very low energies the present cross sections could be several percent higher than for the bare nuclear reaction, depending on the response of the atomic and molecular electrons to the incident beam. We leave to the user of these data the determination of any such corrections for his particular reaction environment, and we have therefore made no shielding corrections to the present data.

We next plan to study both branches of the d + d reaction at low energies and then to undertake measurements of the ^{3}H(t,α)n reaction. Of late, the idea has arisen of using the low-intensity, but energetic, gamma rays produced in some of the pertinent few-body reactions as diagnostics of plasma conditions. It may be possible to investigate such reactions as well at the LEFCS facility.

ACKNOWLEDGMENTS

Many people have contributed to the development of the LEFCS facility. R. Martinez has been especially valuable for his continuing design, construction, and assembly efforts since the project's inception. G. G. Ohlsen and F. D. Correll made major contributions during the early stages of this work, and W. E. Sondheim, L. J. Morrison, and S. E. King also contributed during the early phases. P. A. Schmelzbach aided us in obtaining design information on the calorimeter used at the University of Zürich. R. Hiebert's development and construction of the calorimeter control circuit, and J. W. Toevs's and R. F. Fahlsing's later advice on its operation were invaluable. D. M. Barrus's advice on and J. C Gursky's skill in fabricating the thin foils for the detector ports are greatly appreciated. A. Sabbas assisted us in some data taking and in calculating the backscattering from the calorimeter, and R. E. Cowan furnished us with the accurate calibration resistor for the calorimeter. We thank G. A. Keyworth for obtaining the target system for us from Duke University and for early discussions on its use. W. A. Steyert and K. D. Williamson also furnished useful suggestions about the target cryogenics. D. A. Clark furnished the laser and donated his time and effort for the studies of the time-of-flight method of beam energy measurement. The cooperation of the staff at the Los Alamos Ion Beam Facility has contributed greatly to the success of this project; we especially thank R. Woods, J. Tesmer, L. Rowton, B. Roybal, D. Schmitt, L. Hunt, T. Robinson, D. McMillan, T. Gibson, J. Ross, and R. Poore. We thank G. M. Hale and D. C. Dodder for discussions on the theoretical aspects of this work and for the use of their R-matrix code EDA. M. S. Peacock furnished her usual expert assistance during the computational phases. Mechanical fabrication was ably directed by R. Gill and B. W. Harshman. P. J. Spellman and his collaborators at Sandia Laboratory calibrated our HV resistor stack and digital voltmeters. This work was supported by the U.S. Department of Energy under Contract no. W7405 ENG-36.

[1]N. Jarmie, R. A. Hardekopf, R. E. Brown, F. D. Correll, and G. G. Ohlsen, in *Nuclear Cross Sections for Technology,* edited by J. L. Fowler, C. H. Johnson, and C. D. Bowman (National Bureau of Standards, Washington, D.C., 1980), Special Publication 594, p. 733; N. Jarmie, Nucl. Sci. Eng. 78, 404 (1981); Los Alamos National Laboratory Report LA-8087, 1980 (unpublished).

[2]E. Bretscher and A. P. French, Phys. Rev. 75, 1154 (1949).

[3]H. V. Argo, R. F. Taschek, H. M. Agnew, A. Hemmendinger, and W. T. Leland, Phys. Rev. 87, 612 (1952).

[4]J. P. Conner, T. W. Bonner, and J. R. Smith, Phys. Rev. 88, 468 (1952); J. P. Conner, private communication.

[5]R. G. Jarvis and D. Roaf, Proc. R. Soc. London A218, 432 (1953).

[6]W. R. Arnold, J. A. Phillips, G. A. Sawyer, E. J. Stovall, Jr., and J. L. Tuck, Phys. Rev. 93, 483 (1954); Los Alamos Scientific Laboratory Report LA-1479, 1953 (unpublished).

[7]L. N. Katsaurov, Akad. Nauk. USSR, Trudy, Fiz. Inst. 14, 224 (1962); E. M. Balabanov, I. Ia. Barit, L. N. Katsaurov, I. M. Frank, and I. V. Shtranikh, At. Energ. Suppl. 5, 48 (1957)

[Sov. J. At. En. Suppl. 5, 43 (1958)].
[8]A. P. Kobzev, V. I. Salatskii, and S. A. Telezhnikov, Yad. Fiz. 3, 1060 (1966) [Sov. J. Nucl. Phys. 3, 774 (1966)].
[9]G. M. Hale and D. C. Dodder, in *Nuclear Cross Sections for Technology,* edited by J. L. Fowler, C. H. Johnson, and C. D. Bowman (National Bureau of Standards, Washington, D.C., 1980), Special Publication 594, p. 650; G. M. Hale, private communication. For an earlier evaluation see L. Stewart and G. M. Hale, Los Alamos Scientific Laboratory Report LA-5828-MS, 1975 (unpublished).
[10]S. L. Greene, Jr., Lawrence Radiation Laboratory Report UCRL-70522, 1967 (unpublished).
[11]G. M. Hale, Los Alamos National Laboratory Memo T-2-L-3360, 1979 (unpublished).
[12]L. M. Hively, Nucl. Fusion 17, 873 (1977).
[13]S. Glasstone and R. H. Lovberg, *Controlled Thermonuclear Reactions,* An Introduction to Theory and Experiment (Van Nostrand, New York, 1960).
[14]R. A. Hardekopf, R. E. Brown, F. D. Correll, N. Jarmie, and D. A. Clark, in 1980 Conference on the Application of Accelerators in Research and Industry, Sixth Conference, North Texas State University, 1980, edited by J. L. Duggan and I. L. Morgan, Special Issue of IEEE Trans. Nucl. Sci. NS-28, No. 2, 1339 (1981).
[15]N. Jarmie, R. E. Brown, and R. A. Hardekopf, in *Nuclear Data for Science and Technology,* International Conference, Antwerp, 1982, edited by K. H. Böckhoff (Reidel, Dordrecht, 1983), p. 318.
[16]R. E. Brown, N. Jarmie, and R. A. Hardekopf, in 1982 IEEE Conference on the Application of Accelerators in Research and Industry, Seventh Conference, North Texas State University, 1982, edited by J. L. Duggan and I. L. Morgan, IEEE Trans. Nucl. Sci. NS-30, No. 2, 1164 (1983).
[17]N. Jarmie, R. E. Brown, R. A. Hardekopf, and R. Martinez, in 1982 IEEE Conference on the Application of Accelerators in Research and Industry, Seventh Conference, North Texas State University, 1982, edited by J. L. Duggan and I. L. Morgan, IEEE Trans. Nucl. Sci. NS-30, No. 2, 1508 (1983).
[18]R. A. Hardekopf, G. G. Ohlsen, R. V. Poore, and N. Jarmie, Phys. Rev. C 13, 2127 (1976); R. A. Hardekopf, in *Proceedings of the Fourth International Symposium on Polarization Phenomena in Nuclear Reactions,* Zürich, edited by W. Grüebler and V. König (Birkhäuser, Basel, 1976), p. 865.
[19]P. B. Parks, P. M. Beard, E. G. Bilpuch, and H. W. Newson, Rev. Sci. Instrum. 35, 549 (1964).
[20]G. A. Keyworth II, Ph. D. thesis, Duke University, 1968 (unpublished).
[21]D. M. Barrus and R. L. Blake, Rev. Sci. Instrum. 48, 116 (1977).
[22]E. A. Silverstein, Nucl. Instrum. Methods 4, 53 (1959).
[23]S. E. King and N. Jarmie, Los Alamos Scientific Laboratory Report LA-7999-MS, 1979 (unpublished).
[24]Ch. Thomann and J. E. Benn, Nucl. Instrum. Methods 138, 293 (1976); P. A. Schmelzbach, private communication.
[25]D. C. Kocher and T. B. Clegg, Nucl. Phys. A132, 455 (1969).
[26]N. Jarmie, J. H. Jett, J. L. Detch, Jr., and R. L. Hutson, Phys. Rev. C 3, 10 (1971).
[27]W. S. Chien and R. E. Brown, Phys. Rev. C 10, 1767 (1974).
[28]R. E. Brown, P. M. Hegland, and J. A. Koepke (unpublished).
[29]H. H. Andersen and J. F. Ziegler, *Hydrogen Stopping Powers and Ranges in All Elements* (Pergamon, New York, 1977), Vol. 3 of *The Stopping and Ranges of Ions in Matter.*
[30]S. A. Wender, IEEE Trans. Nucl. Sci., NS-28, No. 2, 1465 (1981); G. Doucas, T. J. L. Greenway, H. R. Mck. Hyder, and A. B. Knox, *ibid.* NS-23, No. 2, 1165 (1976); R. Wilson and G. Brewer, *Ion Beams* (Wiley, New York, 1975); G. Gautherin, C. Lejeune, F. Prangere, and A. Septier, Plasma Phys. 11, 397 (1969); H. Glavish, private communication.
[31]G. G. Ohlsen, R. E. Brown, N. Jarmie, R. A. Hardekopf, S. E. King, F. D. Correll, and D. A. Clark, Bull. Am. Phys. Soc. 24, 822 (1979).
[32]E. M. Burbridge, G. R. Burbridge, W. A. Fowler, and F. Hoyle, Rev. Mod. Phys. 29, 547 (1957).
[33]G. R. Caughlan and W. A. Fowler, Astrophys. J. 136, 453 (1962).
[34]J. N. Bahcall, Astrophys. J. 143, 259 (1966).
[35]D. D. Clayton, *Principles of Stellar Evolution and Nucleosynthesis* (McGraw-Hill, New York, 1968).
[36]C. A. Barnes, in *Advances in Nuclear Physics,* edited by M. Baranger and E. Vogt (Plenum, New York, 1971), Vol. 4, p. 133.
[37]A. M. Lane and R. G. Thomas, Rev. Mod. Phys. 30, 257 (1958).
[38]M. H. Hull, Jr. and G. Breit, *Coulomb Wave Functions,* Handbuch der Physik (Springer, Berlin, 1959), Vol. XLI/1, p. 408.
[39]F. C. Barker, H. J. Hay, and P. B. Treacy, Aust. J. Phys. 21, 239 (1968); F. C. Barker, *ibid.* 25, 341 (1972).
[40]D. C. Dodder, G. M. Hale, N. Jarmie, J. H. Jett, P. W. Keaton, Jr., R. A. Nisley, and K. Witte, Phys. Rev. C 15, 518 (1977).
[41]R. A. Arndt and M. H. MacGregor, in *Methods in Computational Physics,* edited by B. Adler, S. Fernbach, and M. Rotenberg (Academic, New York, 1966), Vol. 6, *Nuclear Physics,* p. 253.
[42]G. M. Hale, in *Neutron Standards and Applications, Gaithersburg, Maryland, 1977,* edited by C. D. Bowman, A. D. Carlson, H. O. Liskien, and L. Stewart (National Bureau of Standards, Washington, D.C., 1977) Special Publication 493, p. 30; G. M. Hale, private communication.
[43]G. H. Miley, H. Towner, and N. Ivich, University of Illinois Report COO-2218-17, 1974 (unpublished); G. H. Miley and H. M. Towner, in *Nuclear Cross Sections and Technology, Washington, D.C., 1975,* edited by R. A. Schrack and C. D. Bowman (National Bureau of Standards, Washington, D.C., 1975), Special Publication 425, Vol. 2, p. 716.
[44]B. H. Duane, in Battelle Pacific Northwest Labs Report BNWL-1685, 1972, edited by W. C. Wolkenhauer (unpublished), p. 75.
[45]E. E. Salpeter, Aust. J. Phys. 7, 373 (1954).